3. PARTICIPATION IN THE USE OF THE JET FACILITIES BY THE EFDA ASSOCIATES

F. Serra (Head), A. Figueiredo, A. Vannucci, B. Gonçalves[1], C. Silva, C. Varandas, D. Alves, D. Borba[2], F. Nabais, F. Salzedas, I. Nedzelski, I. Nunes, J. Sousa, L. Cupido, L. Fattorini, L. Meneses, N. Cruz, M.E. Manso, M.F. Nave, P. Belo, P. Varela, R. Coelho, S. Cortes, S. Hacquin[3], T. Ribeiro, V. Plyusnin.

3.1. INTRODUCTION

The Association EURATOM/IST has proceeded with its participation in the collective use of the JET facilities, in the frame of the "European Fusion Development Agreement" (EFDA) through the "JET Operation Contract" and the "JET Implementing Agreement".

The main activities carried out during this year were related with:

- Operation;
- Scientific exploitation;
- Performance enhancements;
- Management.

3.2. OPERATION

Two members of the IST/CFN staff have been working in the JET Operation Team:

- One physicist belonged to the *"Electron Kinetics Group"*, being responsible by maintenance and data validation of the X-mode correlation reflectometer (KG8b) and the O-mode fluctuation reflectometer (KG3), as well as completing some shifts as "Diagnostic co-ordinator" (DCO) during the restart campaign;
- The other physicist belonged to the *"Operation Group"*, being involved namely in the development of new plasma scenarios and configurations, in particular for the new divertor, and in the conceptual design of the tiles for all the main JET limiters and antenna (ICRH and LHCD) protections, and acting as first Session Leader in the restart of JET (during September/December 2005).

3.3. SCIENTIFIC EXPLOITATION[4]

3.3.1. Introduction

The participation in the JET 2005 Work Programme had contributions from fifteen physicists who performed post-analysis of data from the experimental campaigns C13 - C14, and who were also involved in the preparation of the Campaigns C15-C17. The work was focused on *code developments and physics studies related mainly with Task Forces M (with contributions to S1,S2, and T) , D and E.*

3.3.2. Integration of transport and MHD codes

(i) Implementation of sawtooth models into the transport code JETTO

The so-called sawtooth crash is thought to start with the onset of the m/n=1/1 internal kink mode. During this crash a reconnection process results in the drop of the central temperature. The corresponding outward transport of energy defines an inversion radius that separates the central region, where energy is lost, from an outer region, where energy is deposited.

Until recently the sawtooth physics available in the transport code JETTO was limited to a simple phenomenological model. At a user specified sawtooth crash time, the bulk plasma profiles of density and pressure were flattened within a user specified radius. No redistribution of the magnetic flux was included. In addition, the code could not be used for predictive sawtooth studies since no sawtooth trigger model was available. Following an assessment of available numerical modules, it has been proposed implementing into JETTO: (i) the NTCC Module KDSAW used in TRANSP; and (ii) the Porcelli's sawtooth trigger model available in the BALDUR code. The first part of this work, the implementation of KDSAW into JETTO, has been carried out and completed (Figure 3.1). KDSAW is now fully integrated and tested. A new interface for JAMS has been written. WEB documentation has been prepared. The second part of the work, i.e. the work on the implementation of the Porcelli model was initiated. A test version of JETTO including the Porcelli model is now available.

(ii) Testing JAMS interface for the equilibrium code HELENA and for the MHD code MISHKA[5]

The MHD codes MISHKA and HELENA have recently been integrated into JAMS. However, in order to simplify the JAMS input panels only a limited number of parameters were offered to the user, for the study of edge stability. Test runs of MISHKA and HELENA were

---

[1] Member of the Close Support Unit.
[2] Head of Office for the EFDA Associate Leader for JET
[3] Secondee with JOC.
[4] Work carried out in collaboration with the JET EFDA Contributers

---

[5] Work performed in collaboration with the Association EURATOM/UKAEA, Code Management Group. Contact Person: V. Parail

made to assess the input required in the JAMS interface for the study of core MHD modes. This will be useful for the study of core MHD stability in Optimised shear as well as in ELMy H-mode plasmas. In addition the HELENA and MISHKA codes were tested for the edge MHD analysis of ELM-free discharges with large edge bootstrap currents. Areas for improvement in the input panels, output files and JAMS interface have been identified.
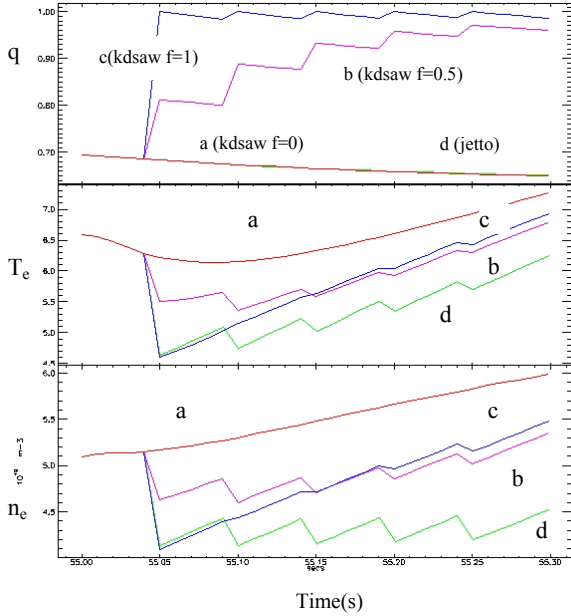

Figure 3.1 – Time traces of central q, T_e and n_e comparing the treatment of sawtooth crashes with KDSAW (curves a (no reconnection), b (partial reconnection) and c (full reconnection)) and the old JETTO (curve d).

3.3.3. JET sawtooth studies
Auxiliary heating be that either from ICRF or NBI has come to be associated with sawtooth stabilization leading to long sawtooth periods. Recent JET experiments challenged our sawtooth knowledge, as observations showed that both types of heating can produce short sawtooth periods, in the range of τ_{ST}=20-100 ms, that are shorter than observed in Ohmic heated plasmas. Experimental results from small sawtooth regimes have continued to be analysed, in particular on sawtooth observations in the reversed B_T campaign. Observations with counter-NBI indicated the important role of rotation on sawtooth stability (Figure 3.2). Two conclusions were made: (i) q-profile modifications from NIB driven current have been excluded as a possible explanation for the different sawtooth observation in co- and counter-NBI; and (ii) qualitatively, the sawtooth period observations may be explained by shear rotation effects on the internal kink stability.

3.3.4 Modelling edge stability of JET quiescent H-mode plasmas
The edge stability of JET QH-mode discharge #59611 has been studied using different versions of the transport code JETTO coupled to an ELM cycle model. Attempts on JET to access the Quiescent H-Mode (QMM) regime with counter-NBI heating, produced plasmas with extended ELM-free phases up to 1.5 s duration. These were characterised by continuous edge n=1 MHD modes similar to the DIII-D "edge harmonic oscillation". The possibility that the edge n=1 mode observed in the QH-mode plasmas may be an external kink mode (similar to the JET Outer Mode observed in Hot-ion H-mode plasmas) is being considered. Different models for the calculation of the Bootstrap Current and Neo-Classical transport were tried (Figure 3.3). A systematic variation of input parameters while searching for continuous ELMs has been made first with the JETTO Default version, then with a JETTO version that is coupled to a Theory Motivated Ballooning/Peeling ELM model. Continuous peeling modes have been obtained with the latter. Sensitivity studies of ELM stability to different edge parameters and to assumptions in the model is in progress. In addition, the edge stability of the n=1 mode is being studied with the codes HELENA and MISHKA.
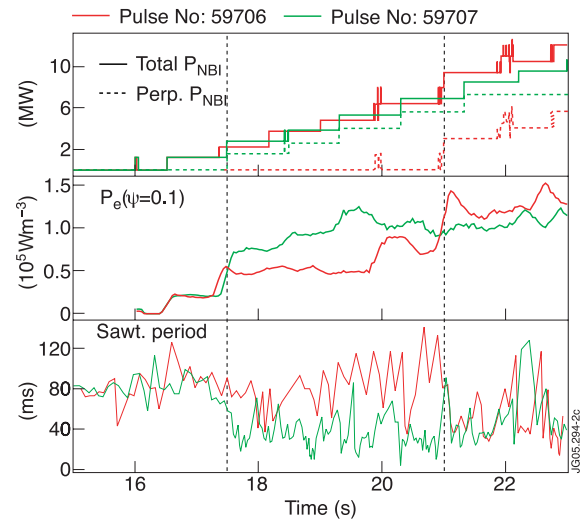

Figure 3.2 – Pair of JET discharges with counter-NBI showing sawtooth periods similar or smaller than observed with Ohmic heating. (a) Total and perpendicular NBI power; (b) Volume averaged power transferred to the electrons, at the flux surface ψ=0.1 (calculated with the PENCIL code); and (c) observed sawtooth period. Vertical lines indicate the times when perpendicular NBI was added: t=17.5 for pulse n. 59707 and t=21 s for pulse n. 59706.
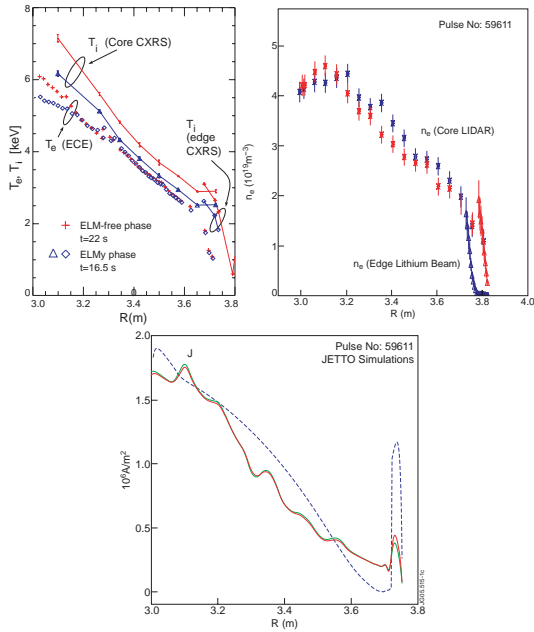
Figure 3.3 - (a) and (b) – Temperature and density profiles measured in a JET Quiescent H-Mode experiment.(c)– Current Density profile modelled with JETTO: (A) Interpretation runs using measured T and n during quiescent phase, for different models for Bootstrap current (Red: NCLASS model, green: JETTO model). (B) Predictive run without ELMs or any other MHD modes (dotted line).

3.3.5. Contribution to DIII-D experiments in the quiescent H-mode (QHM) regime[6]

Current ramps were used to study the stability of edge MHD modes as a function of the plasma current, in quiescent H-mode plasmas. The idea for these experiments originated from a proposal from IST to identify the nature of the Edge Harmonic Oscillator (EHO) and to determine if there were similarities with the MHD observations in JET ELM-free plasmas. It had been proposed that the EHO was likely to be an external kink as the JET Outer Mode and therefore its stability should be sensitive to the edge plasma current. As predicted, the experimental results have shown that the EHO is stabilised by ramping down the plasma current, leading to MHD free periods. In contrast, ramping up the plasma current triggered ELMs. Qualitatively the experiment suggested that the edge of the QHM plasma is marginally stable to external kinks. Both EHO and ELMs behave as external kinks (also known as peeling modes). The EHO observations are consistent with a non-linearly saturated external kink, while the ELMs appear to be linearly unstable external kinks.

3.3.6. Data analysis of n=0 chirping modes observed in JET ion cyclotron heated plasmas.

Persistent rapid up and down frequency chirping modes with a toroidal mode number of zero (n=0) have been observed in the JET tokamak (Figure 3.4). They arise only when

energetic ions with a mean energy ~500 keV are created by high field side ion cyclotron resonance frequency heating. A study of fluctuation data from magnetic and reflectometry diagnostics has been performed.
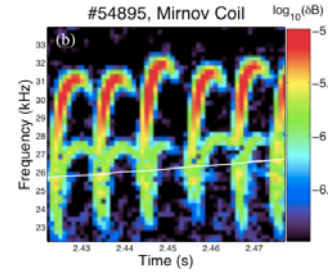

Figure 3.4 – Spectrogram of the signal of a Mirnov coil on JET showing the chirping n=0 mode.

3.3.7. Forecast of tokamak plasma instabilities using artificial neural networks

A research program was initiated to investigate the possibility of using artificial neural networks to forecast the occurrence of major disruptions and ELM instabilities in JET plasmas. The feed-forward neural networks used were chosen to have two hidden layers and were trained using the well known back-propagation algorithm.

Using soft X-ray signals, the major disruptions in some class of plasma discharges could be forecasted up to 2.0 ms in advance, as shown (Figure 3.5). The red and the black curves correspond to the neural network output and to the experimental data, respectively.
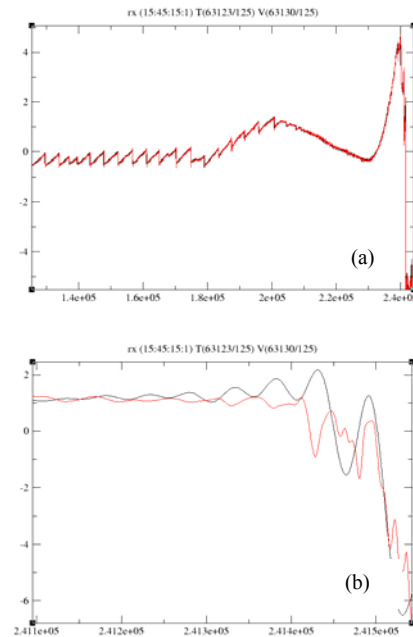

Figure 3.5 – Validation result using JET soft X-ray signal. The red curves represent the output signals from the neural network, forecasted 2.0 ms in advance. In (b) it is shown in detail the last instants of time before the plasma disruption.

---

[6] Work included in the JET collaboration with DIII-D. Contact person: P. West, who led the experiments

Using magnetic signals, both the disruption event and the ELM occurrences could be forecasted up to 1.2 ms in advance. Figure 3.6 presents the comparison the result of the training process (curve in red) to the experimental data (in black). Figure 3.7 shows in detail, an ELM spike and also the plasma disruption event.

After the neural network has been properly trained it was then put to forecast the ELM occurrences and the plasma disruption events using five other different JET plasma pulses. The results obtained can be considered very good, as illustrated in Figures 8 and 9.
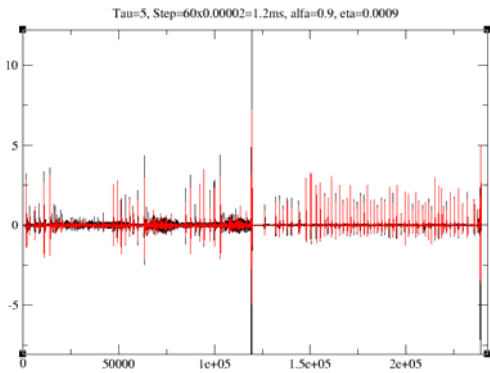

Figure 3.6 – Result of the training process using two JET magnetic signals. The red curve represents the output signals from the neural network, with forecasting time 1.2 ms in advance, and the black curve represent the experimental data.
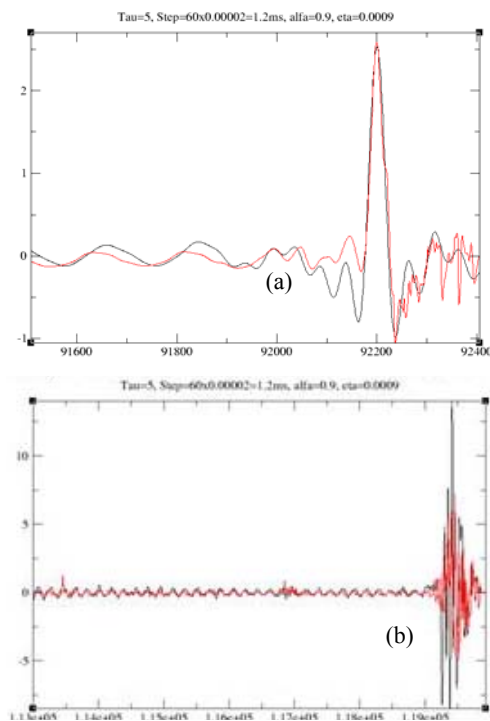

Figure 3.7 – Time expanded signals of figure 6 showing in detail that the neural network closely matches (a) the ELM spike and (b) the plasma disruption event.
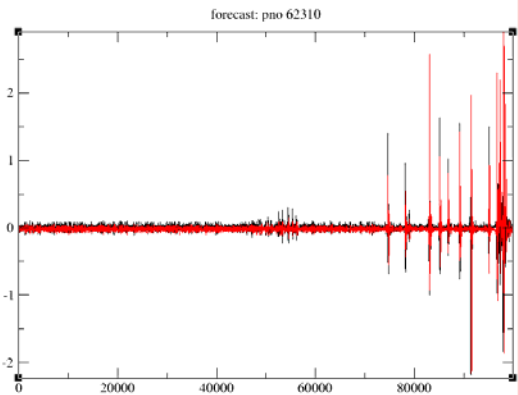

Figure 3.8 – Forecast result (in red) of the JET pulse 62052, using the neural network trained previously. The forecasting time interval is 1.2 ms.
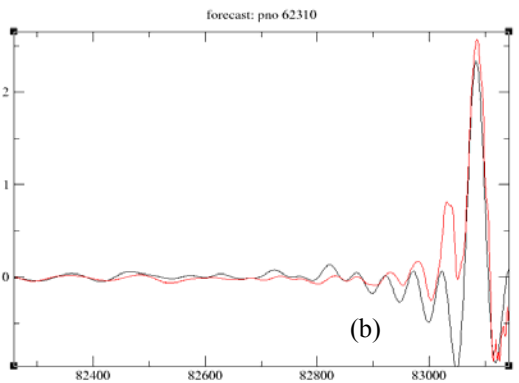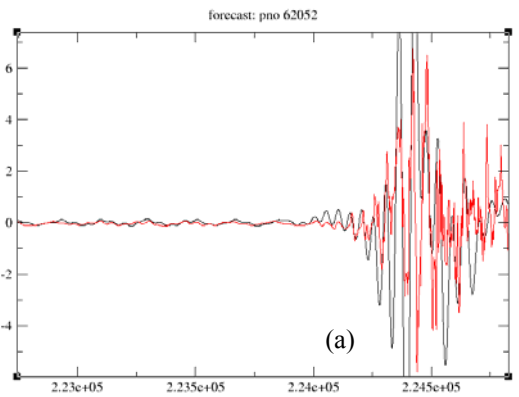

Figure 3.9 – In (a) the disruption event of the JET pulse 62052 (Figure 3.4) is shown in detail. In (b) the time expanded signal of the JET pulse 62310 is presented, showing in detail an ELM spike.

3.3.8. Numerical calculations of the precessional fishbones resonance

A surprising feature of the precessional drift fishbones recently observed in JET low density experiments was its unusually high frequency (around 60 to 90 kHz). To try and explain this, numerical simulations were carried out with the CASTOR-K code. This code allows to calculate the resonant exchange of energy between a mode with an

internal kink structure and populations of ICRH driven fast ions as were used in the experiments. It uses the equilibrium calculated by the HELENA code and the eigenmode calculated by the MISHKA code. Thus, the CASTOR-K code was used to calculate the resonant transference of energy δW_{HOT} between the fast particles population and the mode for different values of T_{HOT}, as function of the mode frequency (Figure 3.10). The modes frequencies that maximize this transference should be around the frequencies observed in the experiments.

Figure 3.10 shows that the best fit between experimental and numerical results is for a fast ions temperature T_{HOT} between 1 MeV and 1.5 MeV, while the value of the fast ions temperature T_{HOT} estimated for these experiments was around 1 MeV. It can also be seen that the mode expected frequency increases rapidly as the fast ions temperature increases. To analyse in more detail what is happening, it is needed an orbits analysis.

Figure 3.11 (upper half) shows the resonant transference of energy between the internal kink mode (f=50 kHz) and three ICRH driven fast ion populations characterized by different temperatures (500, 750 and 1000 keV). The orbits of the particles in stronger resonance with the mode are also represented in Figure 3.11 (lower half). It can be seen that there are two main resonances, one corresponding to particles nearer the magnetic axis centred around 900 keV and the other corresponding to particles farer from the plasma axis centred around 1.8 MeV. This second resonance becomes dominant when the fast ions temperature increases (it is already dominant for T_{HOT}=750 keV). Thus, it can be concluded that there is a change in the type of orbits of the particles that have a stronger interaction with the mode, which cause the mode frequency to increase rapidly with the fast ions temperature and may explain the high frequency of the precessional fishbones observed experimentally.

3.3.9. Improved time–frequency visualization of chirping mode signals in tokamak plasmas using the Choi-Williams distribution

The use of auxiliary heating in tokamak plasmas produces energetic ions that can destabilize a variety of magnetohydrodynamic (MHD) modes. These instabilities may expel energetic ions from the plasma core, reducing the heating efficiency. Often, such MHD instabilities have time-varying frequencies, being referred to as "chirping modes". The best examples are "fishbones", which have decreasing frequency while the mode amplitude increases. Such chirping down has also been observed in JET Alfvén eigenmodes. Upward frequency chirping is less common, although sometimes observed in JET plasmas with ion cyclotron resonant heating (ICRH).

Here, it is shown an unusual class of JET low-frequency chirping modes, with toroidal mode number n = 0, which are rapidly swept upwards and downwards in the 25–40 kHz range. Similar nearly symmetric up and down chirping has recently been observed in toroidal Alfvén eigenmodes in the spherical tokamak MAST with neutral beam heating. The nonstationary character of MHD chirping modes is best seen in a time–frequency image, which can be compared with others from nonlinear theoretical models of kinetic instabilities. These models predict frequency splitting as well as frequency sweeping. The short-time Fourier transform spectrogram has been used to analyze chirping mode signals. Still, images based on the spectrogram are hindered by a trade-off between time and frequency resolution, which is particularly detrimental when nonstationarity is strong. Excellent time–frequency resolution can be achieved with the Wigner distribution, but artifacts may preclude its use for signals with multiple components. The Choi-Williams distribution allows a compromise to be made between good time–frequency resolution and an acceptable level of artifacts.
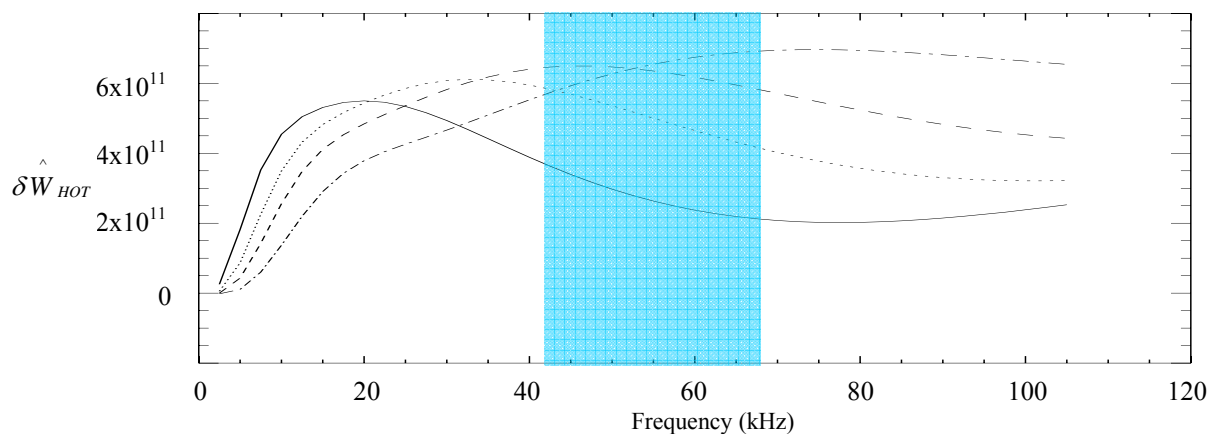

Figure 3.10 - Resonant transference of energy between the internal kink mode and an ICRH driven fast ions population with temperatures of 500 keV (solid line), 750 keV (dotted), 1 MeV (dashed) and 1.5 MeV (dashed/dotted). The observed frequency of precessional fishbones is shadowed.
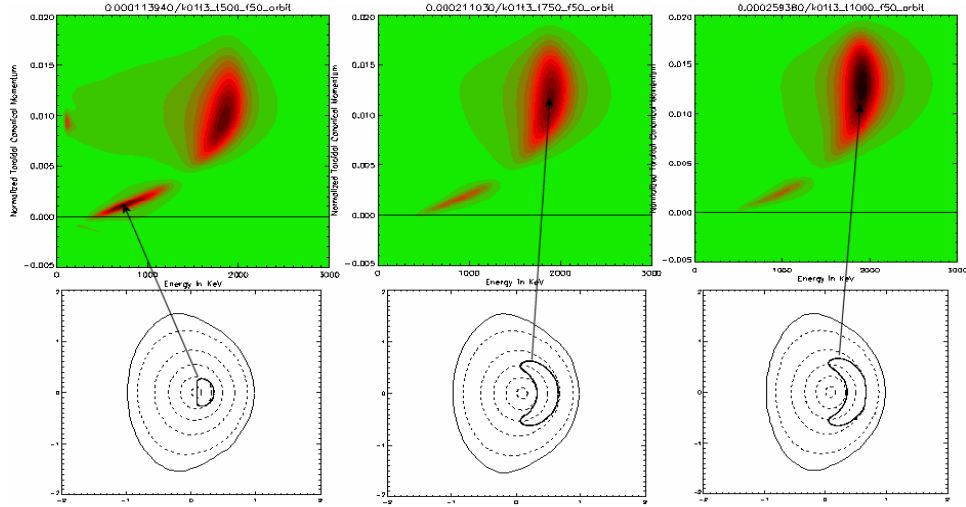
Figure 3.11 - Upper line - Resonant transference of energy between the internal kink mode (f=50 kHz) and an ICRH driven fast ions population as function of the energy and the toroidal canonical moment for three different fast ions temperatures: 500 keV (left), 750 keV (middle) and 1000 keV (right). Lower line: Orbits of the particles with a stronger interaction with the node, for each case.

The images in Figure 3.12 are time–frequency representations of chirping modes in a JET plasma, which are observed during the initial heating phase — when ICRH is applied — of a discharge with a non-monotonic current density profile. Figure 3.12 shows that the Choi-Williams distribution does yield a sharper time–frequency picture than the spectrogram. Artifacts can be recognized in Figure 3. 12(a) by their oscillatory nature, but pose no problems reading the plot since they are separated from the signal components. In Figure 3.12(b), the spectrogram shows each burst of magnetic activity as a pair of modes that start at the same low frequency and then diverge with one mode chirping up and the other chirping down. In Figure 3.12(a) the frequency splitting in two modes is more clearly observed even at the lowest frequency.
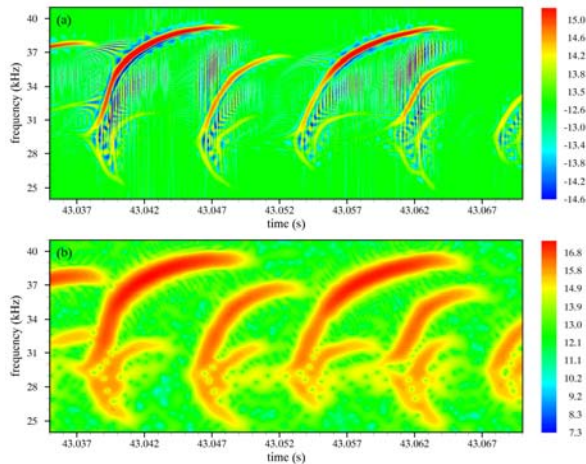

Figure 3.12 - Time–frequency density plots of a chirping mode signal (JET pulse 54893) obtained using (a) the Choi-Williams distribution with $\sigma = 25$ and (b) the spectrogram with a 2 ms window.

3.3.10. Impurity transport studies

The classical friction in the SOL was studied as a mechanism to prevent impurities to reach the plasma core. A 2-D multispecies transport code EDGE2D/NIMBUS was used, for typical MARKIIGB divertor H-mode JET plasmas. To describe H-mode plasma we used a prescribed ad-hoc perpendicular transport coefficients of heat and particle diffusivities, and drifts were not considered. The parallel transport was determined using the 21 moments approximation of the Braginskii equations .

The force balance between the classical parallel friction force and the thermal force are related to Neon content inside the last closed flux surface. The higher is the friction force relatively to the thermal force the lower is the Neon content in the core before the plasma detachment. This study was done for four different main gas inlet positions: top of the vessel, divertor region, inner mid plane and outer mid plane. We found that Neon exhaust is better for the latter case. This conclusion is still valid with the change of impurity boundary conditions although some differences are found: the plasmas detaches at higher densities because the electron temperature at the inner divertor is higher and the Neon enrichment factor is lower because the system allows more impurities inside the last closed flux surface for the steady state boundary condition, $\nabla n_z(\psi_{min}) = 0$, than for the external impurity puff $n_z(\psi_{min}) = 0$ (Figure 3.13).

The Neon core content is lower and the enrichment factor is higher for the simulations with Neon and Carbon than with Neon only but for main ion densities at the plasma detachment. The main influence of Carbon on Neon is the plasma detachment onset happens at lower main ion densities. There is no clear increase of the friction force between Carbon and Neon. The sum of

friction and the thermal forces is lower and closer to zero at onset of plasma detachment making the Neon to be mainly confined in the divertor region in such plasma.
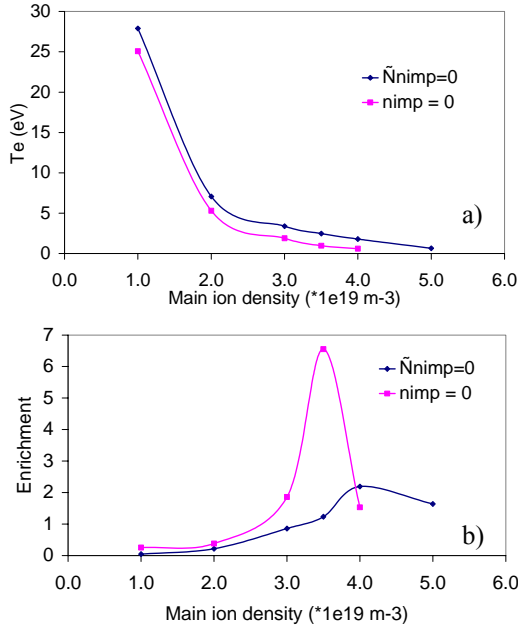

Figure 3.13 - a) Electron temperature at the inner divertor and b) Neon enrichment factor for the two boundary conditions at the last closed flux surface.

A reduction of the core carbon content and a drop of the C^{2+} spectral line intensity in the divertor region were observed in high density seeded impurity JET plasmas after the introduction of the extrinsic impurity . We found the same effects in our simulations with Carbon and with Carbon and Neon of the experiments when we compare the modelling results for the same main ion densities. However these effects are also observed in a pure Carbon simulation but at higher main ion densities, (Figure 3.14). We can conclude that the extrinsic impurity plays an indirect role on the Carbon redistribution and it is the electron temperature in the divertor region that is the main factor. Namely it is the reduction of the electron temperature that leads to and increase in the friction force relatively to the thermal force. As the plasma approaches detachment the electron temperature becomes so low that the efficiency of the carbon chemical sputtering goes down reducing the C^{2+} spectral line intensity in the divertor region (Figure 3.15).

3.3.11. Exploitation of the microwave reflectometry systems[7]
(i) Characterisation of Alfvén Cascades (ACs) in advanced plasma regimes
The excitation and observation of Alfvén Cascades are now used to diagnose advanced plasma scenarios with
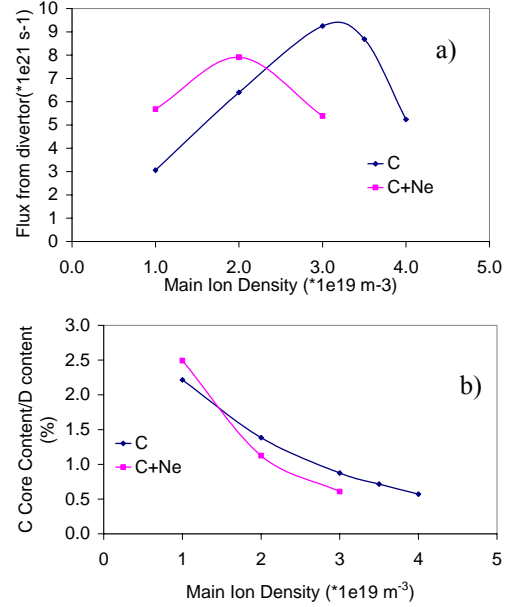

Figure 3.14 - a) Carbon source at the divertor and b) carbon content inside the last closed flux surface / deuterium content, for the simulations with carbon (c) only and with carbon + Neon (c+Ne).
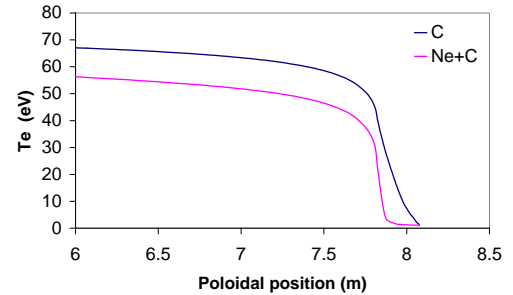

Figure 3.15 – Electron temperature along a poloidal field line 1 cm outside the last closed flux surface, in the SOL of the inner divertor for simulations with C and Ne+C.

Internal Transport Barriers (ITBs). In addition to the determination of the reversed magnetic shear, the time evolution of the safety factor minimum $q_{min}(t)$ can be inferred from the time evolution of the Alfvén Cascade frequency. A good determination of $q_{min}(t)$ is crucial for the development of such scenarios on JET since the ITBs are usually triggered at low order rational magnetic surfaces corresponding to $q_{min}(t)$. The JET O-mode multi-channel reflectometer (KG3 diagnostic) used in the interferometry regime allows routine measurement of Alfvén Cascades with high frequency and time resolution. In addition, the level of density fluctuations induced by an Alfvén Cascade can be inferred from the phase perturbations of the reflectometry signal. This only requires an assumption on the shape of the density fluctuations, which can be obtained from an equilibrium

reconstruction and MISHKA-H and NOVA-K computations. The level of density fluctuations is then estimated by matching the phase perturbations evaluated experimentally (Figure 3.16) and those computed by WKB simulations.

(ii) Turbulence studies

H-mode access at very low plasma density has been studied on JET, providing valuable information on the physics of the edge transport barrier formation . In particular, a significant reduction of the turbulence level was observed after the L-H transition (Figure 3.17). This is exemplified on the figure below, which displays a clear reduction of the fluctuations of the reflectometer signal reflected in the edge plasma region.
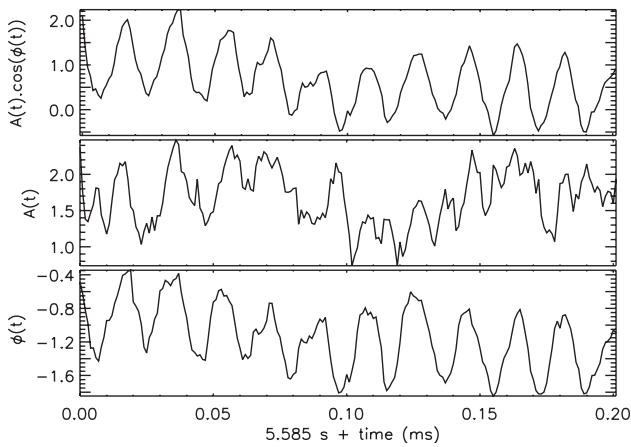

Figure 3.16 - Fluctuations of the reflectometry homodyne signal, of its amplitude and of its phase induced by the presence of an Alfvén cascade
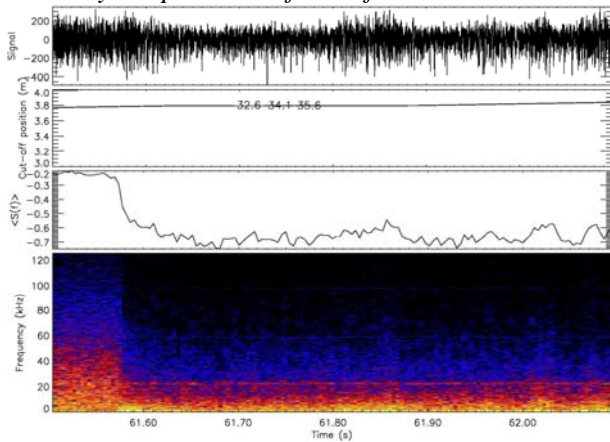

Figure 3.17 - Reduction of plasma turbulence at the L-H transition observed from a O-mode reflectometry signal at fixed frequency 34.1 GHz. From upper to lower parts: Raw reflected signal (b) Radial position of the cut-off layer (c) Averaged level of the reflected signal fluctuations (d) Spectrogram (sliding FFT) of the reflected signal

3.3.12. Turbulence experiments in reversed and standard-B field configurations in the JET tokamak

In 2005 it was performed the analysis of the data collected by the fast reciprocating Langmuir probe system in the plasma boundary region during the campaigns of 2003/2004 with the aim to compare plasma turbulence in normal and reversed field configurations. Basic turbulence properties (e.g. level of fluctuations, ExB turbulent transport) are comparable in normal and reversed field configurations. It was observed that the SOL turbulence is less intermittent in REV-B discharges.

The normalized Probability Distribution Function (PDF) shows that the distributions of fluctuations in the ion saturation current, I_s and the floating potential, V_f are very similar in both magnetic field directions (Figure 3.18). It should also be noted that the PDF's were obtained at different radial positions. Some differences in PDF shape are observed for the measurements from the far SOL (star points).

The normalized PDFs of the turbulent flux are also remarkably similar (Figure 3.19). A reduction of the intermittence is observed in REV-B discharges (closed symbols) being this reduction more pronounced in inward intermittent flux events ($\Gamma_{ExB} < -5 <\Gamma_{ExB}>$, negative tail of the curve). This small difference is not reflected in the turbulent flux profiles because the contribution from intermittent events to the total flux is small.
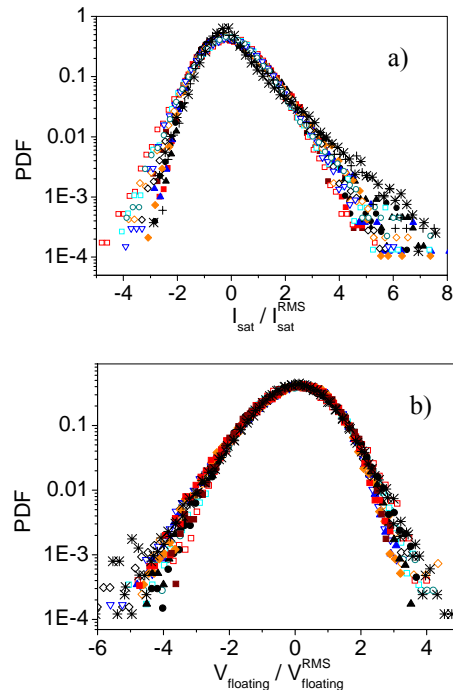

Figure 3.18 - Probability Distribution function of I_s (a)) and V_f (b)) normalized to the level of fluctuations
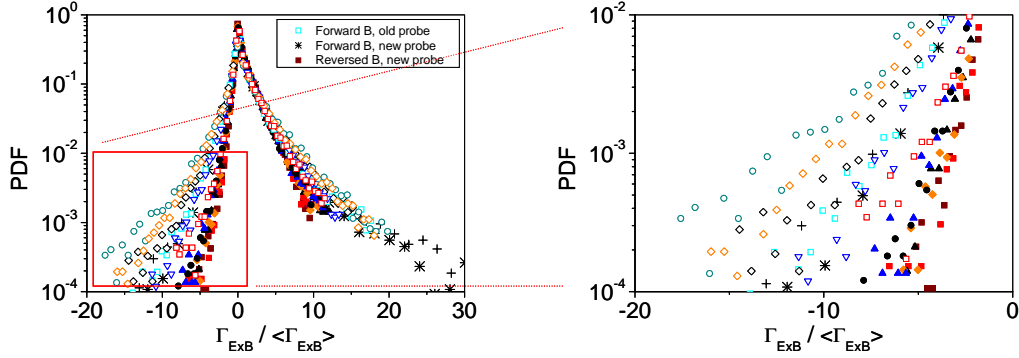
Figure 3.19 - a) PDF of the turbulent ExB flux. b) A detail of the tail of the distribution shows a reduction in the inward intermittent events for the reversed field discharges.

3.3.13. Analysis of generation and loss mechanisms of runaway electrons

A comprehensive understanding of the trends of disruption-generated runaway electrons (REs) is needed to avoid their detrimental consequences on the materials of the plasma facing components (PFC) and vacuum chamber in large tokamaks and ITER. Comparison of experimental results and numerical modeling has allowed further contribution into development of the model for generation of runaway electrons during disruptions. Numerical modelling has been carried out in frame of a test particle model taking into account the evolution of the runaway beam geometry, which has been observed in experiments using soft-X diagnostics. A detailed scan on RE beam size shows that calculated current conversion efficiency can exceed the upper bound of the experimental values if the RE beam will occupy the whole plasma cross-section despite a significant decrease of the RE density (Figure 3.20 (a,b,c)). At some combinations of the disruption parameters the current conversion rate can achieve 100%, which never has been observed in experiments. Similar trends have been also predicted by other studies, where under certain conditions practically all the initial plasma current can be converted into runaways.

Several mechanisms are considered as possible reasons for the observed in experiments a 60% upper bound for the current conversion rate:

(i) REs are sensitive to magnetic fluctuations, which decrease the characteristic life-time of the runaways: $\tau_{RE}=a_{pl}/5.8D_r$, where $D_r \approx \pi q R_0 c (b_r/B_0)^2$ is the coefficient of the radial diffusion caused by the presence of magnetic field perturbations with the magnitude b_r. Very large magnetic perturbations lead to the enhanced losses of fast particles and limit the energy and total amount of REs at the early stage of disruptions. However, with the increase of kinetic energy (W_{kin}) REs become less sensitive to the magnetic turbulence.

(ii) Another loss mechanism can be understood from the analysis of the runaway orbit outward drift as the RE energy increases: $d_r=c/\omega_{ce} (q/P_\parallel)(P_\parallel^2 + P_\perp^2/2)$. From this expression one can obtain a condition for the energy of runaway electron, at which it will escape outside the confining region

created after disruption: $P_\perp^2=2(d_r/q*\omega_{ce}/c*P_\parallel-P_\parallel^2)$ (Figure 3.21 (a)). So, that even under conditions of the perfect confinement the runaway electrons can produce intense photo-neutron emission interacting with PFC due to outward shift of the runaway orbit at certain values of the REs energy (Figure 3.21 (b)).
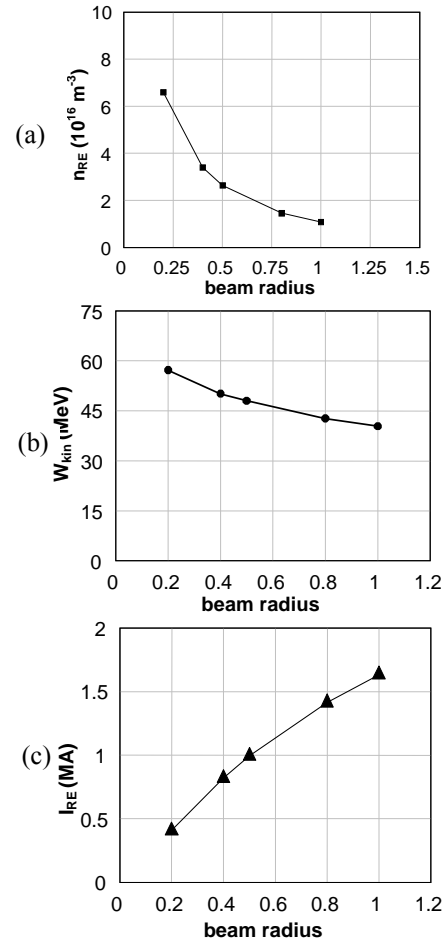

Figure 3.20 - Dependence of the calculated RE density (a), maximal kinetic energy (b), and RE currents vs. dimensionless runaway beam radius.
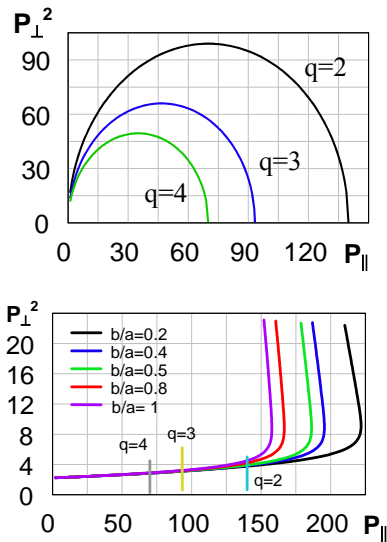
Figure 3.21 - (a) - Trajectories of the test electron in a momentum space at which its orbit outward shift becomes equal to the minor plasma radius ($d_r=a$, for $a=1$ m) at different values of safety factor: $q=2,q=3$ and $q=4$. (b) - Evolution of the test runaway electron at different values of dimensionless runaway beam radius. Conditions for complete runaway electron diffusion from the confining region are presented by curves calculated at values $q=2,3$ and 4.

3.4. ENHANCEMENTS
3.4.1. Introduction
The Association EURATOM/IST has been in charge with the following tasks carried out in the frame of the JET Enhanced Performance Project:
- Mw access – Project management and implementation;
- Development of a new fast sweep frequency reflectometer;
- TOFOR – Project design and procurement activities;
- Collaboration in the commissioning of TOFOR and MPRu;
- RTP – Development of a real-time test facility;
- PCU-VS – design of the PCU vertical stabilization;
- DPDT4 – Real-time measurement & control diagnostics & infrastructure project;
- Fast wave reflectometer.

3.4.2. Millimeter wave access (EFDA/01-625)
The installation of both *in-vessel and ex-vessel hardware*, namely antennas and waveguides for both reflectometry and ECE, was completed. A *quasi optical coupling arrangement* to couple five different systems into a waveguide was developed. Calibration of the existing *correlation reflectometrs* to the expected performance within the new waveguides was done.

Tests were performed, first with a mirror in-vessel and later with plasma.

Figure 3.22 shows that significant improvements of the S/N ratio for the KG8b reflectometer signals have been reached. The increase of the raw signal amplitude by a factor of 50 suggests an improvement of at least 17 dB and a clear dynamic can now be observed on the signal spectrum**.**
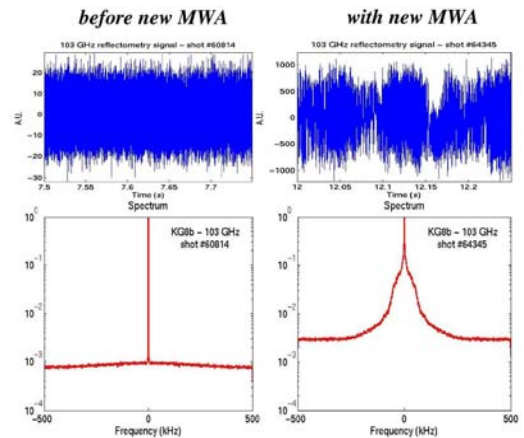

Figure 3.22 - Raw signal and corresponding spectrum from the KG8b 103 GHz channel before (on the left) and after (on the right) the installation of the new MWA

3.4.3. Development of a new fast swept frequency reflectometer (KG8a diagnostic).
A *new fast swept-frequency heterodyne reflectometer* (KG8a diagnostic) dedicated to density profile measurement is being developed and should be operational for the next JET experimental campaigns in 2006. Providing routine measurement of the edge density profile with high spatial (< 1 cm) and temporal (< 30-50 μs) resolution, this diagnostic will be of the greatest importance for the pedestal studies on JET. In addition to the development of the routine for density profile inversion, some theoretical studies were carried out in order to estimate the spatial resolution of these measurements. The influence of the misalignment between the plasma magnetic axis and the probed region was especially assessed. As depicted in the figure below, a spatial resolution better than 1 cm is expected from the KG8a measurements in a large majority of the JET discharges.

3.4.4. TOFOR – Project design and procurement activities[8]
Five *time digitizer boards* (TDB) were assembled and delivered to JET after successfully tested at the Uppsala University. Since the TDB power needs require that no more than three boards coexist in the same computer, the *control software* was modified for three plus two boards in two computers, with an implementation of a TCP

---

[8] Work carried out in collaboration with the Swedish Euratom Association
Contact Person: J. Kelme

based synchronism server and a client. Better synchronization links were tested and found operative for the required length. Integration of the boards in the diagnostics was performed by the VR Association in close collaboration with IST/CFN.
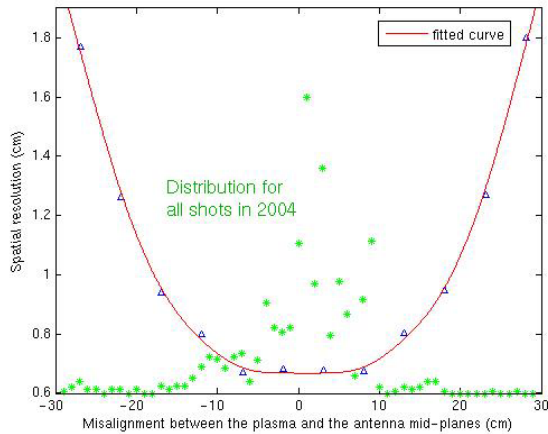

Figure 3.23 - Estimation of the spatial resolution of the KG8a reflectometer diagnostic as a function of the misalignment between the plasma and the reflectometry antenna mid-planes

3.4.5. RTP – Development of a real-time test facility
The *complete unit providing 32 waveform generator (WG) plus 8 transient recorder channels* was assembled. Requirements compliance tests were performed at IST/CFN. Integration to CODAS and functional tests were performed at JET by the IST/CFN staff with success. Minor accuracy corrections on the WG outputs and additional software features allowing local unit control were incorporated. Software and hardware manuals have been finished.

3.4.6. PCU-VS – Design of the PCU vertical stabilization
The implementation of a new vertical stabilization controller will require the increment of the number of input signals to over 50, while maintaining the control loop delay under 50 μs, and aiming to reducing it to fewer than 10 μs. The design of an *ATCA-based hardware platform (Figure 3.24) for the low-latency controller* was proposed aiming at:

- Reducing the delays on the acquisition/generator endpoints and data interconnect links;
- Providing high processing power near the acquisition/generator endpoints and on the system controller;
- Providing the synchronism of all digitizer/generator endpoints;
- Having an architecture designed for maintainability, upgradeability and scalability;
- Targeting the specificities of the VS controller including low cost per channel;
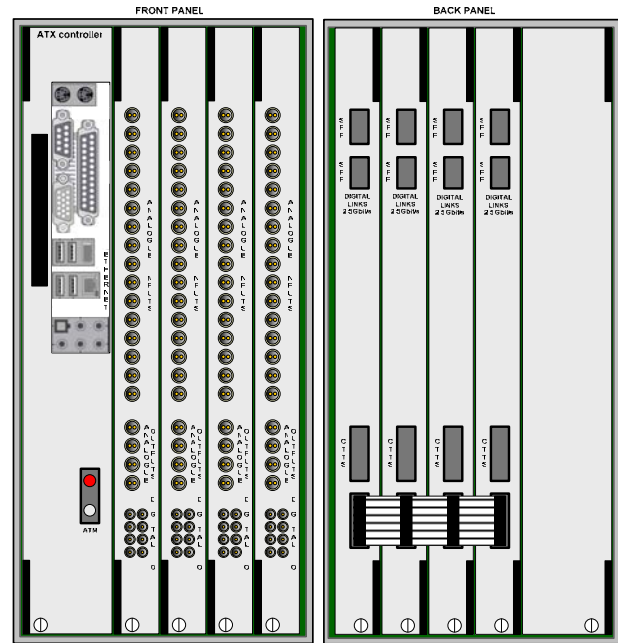- Decreasing risks during implementation and testing.

Figure 3.24 - Vertical stabilization controller

3.4.7. DPDT4 – Real-time measurement & control diagnostics & infrastructure project
The essential aim of this project is to expand JET real-time diagnostics and control capabilities required to fulfil the programme objectives of JET in the proposed FP7 phase of operation dedicated to ITER preparation. In particular the objective is to optimize the control of the plasma during operation and to enable control schemes for the main plasma scenarios and in particular profile control. In response to the call for participation in the diagnostic enhancements, Associations IST, CEA and UKAEA declared interest in the project. IST offered to lead the project and proposed the workgroup organization chart of Figure 3.25.

3.5. Management
The Association EURATOM/IST has collaborated on the management of the use of the JET facilities by the EFDA Associates in the following manner:

- Dr. Duarte Borba, as Head of Office for the EFDA Associate Leader for JET,
- Dr. Bruno Gonçalves as a member of the staff of the Close Support Unit to the EFDA Associate Leader for JET;
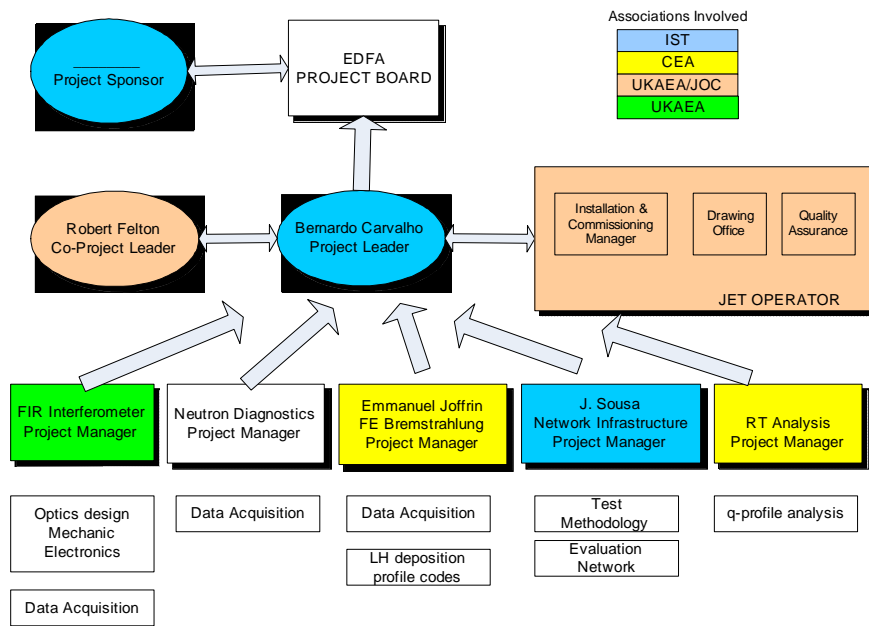- Prof. Horácio Fernandes and Dr. Paulo Varela as members of the Remote Participation Users Group.

Figure 3.25 – Organization of the DPDT4 project